


 Cite this: *RSC Adv.*, 2023, **13**, 27782

# Perovskite SrZrO<sub>3</sub>:Ho<sup>3+</sup> phosphors: synthesis, structure, Judd–Ofelt analysis and photoluminescence properties

 Vijay Singh \*<sup>a</sup> and M. Seshadri<sup>b</sup>

A series of SrZrO<sub>3</sub>:xHo<sup>3+</sup> (x = 0.01, 0.03, 0.05, 0.07, 0.09, and 0.11 mol) perovskite phosphors have been synthesized by using the sol–gel technique. The structural and optical characteristics of the prepared phosphors have been investigated through powder XRD, FT-IR, UV-visible diffuse reflectance, and photoluminescence analysis. The photoluminescence emission spectra showed a bright characteristic peak at 545 nm (<sup>5</sup>F<sub>4</sub> + <sup>5</sup>S<sub>2</sub> → <sup>5</sup>I<sub>8</sub>) under the 454 nm excitation, which exhibits emission in the green region of the electromagnetic spectrum. The emission intensity of the phosphors starts decreasing slowly beyond 3 mol% Ho<sup>3+</sup> ions concentration due to concentration quenching, which is attributed to the dipole–dipole interaction between Ho<sup>3+</sup> ions. The site symmetry of the Ho<sup>3+</sup> ions has been studied by estimating the relative Judd–Ofelt intensity parameters (Ω<sub>λ</sub>, where λ = 2, 4, 6) from the photoluminescence excitation spectrum of the SrZrO<sub>3</sub>:0.03Ho<sup>3+</sup> phosphor. The obtained findings suggest that the synthesized phosphors will be favorable for their bright green emission and thus, can be widely used for different optoelectronic applications.

 Received 21st June 2023  
 Accepted 7th September 2023

DOI: 10.1039/d3ra04175a

[rsc.li/rsc-advances](https://rsc.li/rsc-advances)

## 1. Introduction

Perovskite materials with the general formula ABO<sub>3</sub> (where A = Ca, Sr, Ba; and B = Zr, Hf, Ti) have great versatility and outstanding chemical, physical, electrical, and thermo-mechanical properties. These host lattices are getting special attention due to their potential applications as catalysts, photocatalysts, fuel cells, in photovoltaic applications, optoelectronics, and solid oxide fuel cells.<sup>1–3</sup> Perovskite materials possess a fascinating feature in which a slight variation in structure and chemical composition may result in enormous changes in their chemical and physical properties.<sup>4–7</sup> The doping of a foreign element into these ABO<sub>3</sub> type inorganic oxides influences their optical and magnetic properties by creating various defects.<sup>8,9</sup> Especially, lanthanide ions as dopants are suitable candidates since they exhibit unique spectroscopic properties.<sup>10–12</sup> The coordination geometry and oxidation states of uranium ions in the SrZrO<sub>3</sub> perovskite were studied by Gupta *et al.*,<sup>13</sup> although Li *et al.*<sup>14</sup> investigated the spectral characteristics and intrinsic defects of SrZrO<sub>3</sub> perovskite. The earlier report published by Knight *et al.*<sup>15</sup> reveals the structural and thermoelastic characteristics of SrZrO<sub>3</sub> perovskite.

Perovskites have been reported to be advantageous in high-temperature applications, like hydrogen gas sensors, steam

electrolysis, and fuel cells.<sup>16–18</sup> Proton conductivity at elevated temperature enables its usage in typical electrochemical devices. Among different perovskite materials, the SrZrO<sub>3</sub> host material has been suggested for use as a potential substrate due to its large single crystals.<sup>19</sup> In recent years, the structural phase transitions of strontium zirconate perovskites have been studied significantly at room temperature and higher temperatures.<sup>20–22</sup> Initially, the structural investigations revealed that the SrZrO<sub>3</sub> possesses an orthorhombic phase at room temperature, and later Carlsson<sup>23</sup> proposed the presence of additional phases at high temperatures. Mete *et al.*<sup>17</sup> examined the structural and electronic characteristics of 4d-perovskite: the cubic phase of SrZrO<sub>3</sub>. The electronic and structural performances of selected surfaces of SrZrO<sub>3</sub> were investigated by Sambrano *et al.*<sup>24</sup> Singh *et al.*<sup>25</sup> have also published research on the photoluminescence and structural properties of SrZrO<sub>3</sub>:Sm<sup>3+</sup> orange-emitting perovskite phosphors.

Due to long-lived excited states and energy levels, the trivalent lanthanide ions doped luminescent materials (using Tm<sup>3+</sup>, Er<sup>3+</sup>, and Ho<sup>3+</sup> ions) have been selected as the main subject of interest by several research groups.<sup>26–28</sup> Holmium belongs to the lanthanides and its electronic configuration becomes [Xe]4f<sup>10</sup> when doped into a crystalline host. Several spectroscopic studies revealed that Ho<sup>3+</sup> is the most desirable ion for mid-infrared lasers and has excellent green emission properties other than Tb<sup>3+</sup> (green emission only) ions among the rare earth ions due to its various electronic transitions. Ranjan *et al.*<sup>29</sup> reported the enhanced green up-conversion emission of Ho<sup>3+</sup> doped Gd<sub>2</sub>O<sub>3</sub> phosphor by co-doping with Yb<sup>3+</sup> ions. The luminescence studies of Eu<sup>3+</sup> and Ho<sup>3+</sup> doped Sr<sub>2</sub>TiO<sub>4</sub> revealed

<sup>a</sup>Department of Chemical Engineering, Konkuk University, Seoul 05029, Republic of Korea. E-mail: vijayjiin2006@yahoo.com

<sup>b</sup>Department of Physics, Koneru Lakshmaiah Education Foundation, Hyderabad 500043, Telangana, India


that the  $\text{Sr}_2\text{TiO}_4$  could be a suitable material in favor of high-pressure mercury vapor lamps or white light-emitting diodes.<sup>30</sup>

A literature survey confirms a lack of reports available on  $\text{Ho}^{3+}$  doped  $\text{ABO}_3$  type zirconate perovskites. The  $\text{Ho}^{3+}$  is often used as a structural probe because it can be accommodated at the A-place or B-place of perovskite oxides and in-site changes in the optical behavior and local site surrounding these doped oxide materials. Based on these results, our prepared sample possesses excellent thermal and chemical stability, prompting its practical application. Combining trivalent rare-earth metal ions in zirconate perovskites is considered as a promising approach to developing more useful and stable luminescent materials. Shi *et al.*<sup>31</sup> prepared  $\text{Yb}^{3+}$ ,  $\text{Ho}^{3+}$ ,  $\text{Li}^+$  tri-doped  $\text{TiO}_2$  up-conversion materials to enhance the efficiency of perovskite solar cells. First, Hou *et al.*<sup>32</sup> investigated the impacts of  $\text{Ho}^{3+}$  ion doping over the surface morphology, crystal phase, and magnetic characteristics of  $\text{BiFeO}_3$  thin films synthesized by the sol-gel technique. Sharif *et al.*<sup>33</sup> investigated surface morphology, structural, magnetic, and dielectric properties in

the  $\text{BiFeO}_3$  with holmium-doped thin films deposited by the pulsed laser deposition technique. Moreover, Hussain *et al.*<sup>34</sup> presented resistive leakage and intrinsic polarization analyses for high-performance piezo/pyroelectric  $\text{Ho}$ -doped  $0.64\text{Pb}(\text{Mg}_{1/3}\text{Nb}_{2/3})\text{O}_3$ - $0.36\text{PbTiO}_3$  binary ceramic materials.

Besides the solid-state reaction process, a conventional synthetic route for preparing phosphor particles, several new synthetic methods have already been developed, for example, co-precipitation, sol-gel, solution combustion, microemulsion, spray pyrolysis, and hydrothermal synthesis. The present work uses the sol-gel method to prepare  $\text{SrZrO}_3$  phosphor. Sol-gel is a synthetic route to synthesize ceramic oxides, which provides reasonable control over stoichiometry, high purity, good homogeneity, and reduced sintering temperature. This method may also enable the production of low-temperature phases. A sol-gel method in a liquid includes a polycondensation reaction, which builds the oxide network of a molecular precursor. Although the process consists of several steps, doping concentration positively impacts the luminescence and crystal structural properties of the prepared phosphor. Wurm *et al.*<sup>35</sup> prepared sol-gel  $\text{SrZrO}_3$  and  $\text{SrTiO}_3$  coatings on C and SiC-fibers. Venkatesh *et al.*<sup>36</sup> prepared a novel strontium zirconate perovskite coating on an Inconel substrate using the sol-gel synthesis method. Liu *et al.*<sup>37</sup> reported sol-gel derived  $\text{SrZrO}_3$  memory thin films with resistance switching properties. In this work, the  $\text{Ho}^{3+}$  doped  $\text{SrZrO}_3$  perovskite phosphors were synthesized by using sol-gel synthesis. The prepared phosphors were characterized structurally and optically. To know the spectral characteristics, the measured photoluminescence excitation spectra were used to calculate the Judd-Ofelt intensity parameters,  $\Omega_2$ ,  $\Omega_4$  &  $\Omega_6$ . Detailed photoluminescence properties are discussed herein.

Table 1 Detailed information of sample composition and starting materials

Sample compositions	Weight of starting materials (g)			
	$\text{Sr}(\text{NO}_3)_2$	$\text{ZrO}(\text{NO}_3)_2 \cdot 2\text{H}_2\text{O}$	$\text{C}_6\text{H}_8\text{O}_7$	$\text{Ho}(\text{NO}_3)_3 \cdot 5\text{H}_2\text{O}$
$\text{SrZrO}_3:0.01\text{Ho}$	0.8464	1.0688	3.0738	0.0176
$\text{SrZrO}_3:0.03\text{Ho}$	0.8464	1.0688	3.0738	0.0592
$\text{SrZrO}_3:0.05\text{Ho}$	0.8464	1.0688	3.0738	0.0882
$\text{SrZrO}_3:0.07\text{Ho}$	0.8464	1.0688	3.0738	0.1243
$\text{SrZrO}_3:0.09\text{Ho}$	0.8464	1.0688	3.0738	0.1578
$\text{SrZrO}_3:0.11\text{Ho}$	0.8464	1.0688	3.0738	0.1940

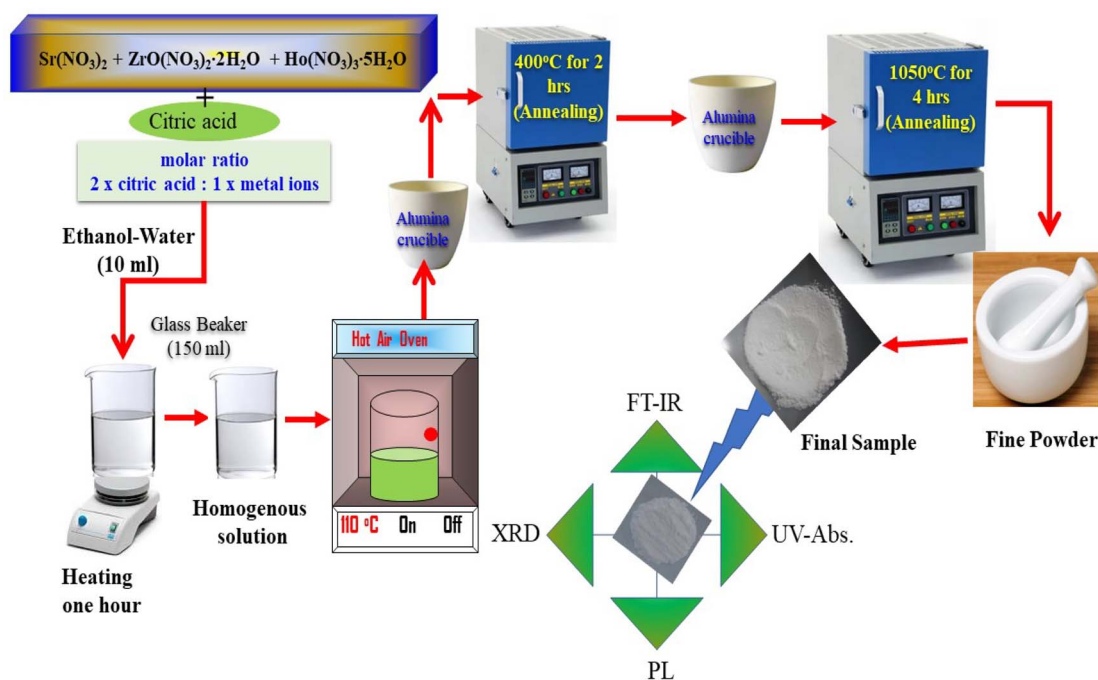


Fig. 1 Systematic diagram of synthesis process of the sample.



## 2. Materials preparation and analysis

The  $\text{SrZrO}_3:x\text{Ho}^{3+}$  ( $x = 0.01, 0.03, 0.05, 0.07, 0.09, \text{ and } 0.11 \text{ mol}$ ) perovskite phosphors were fabricated by sol-gel procedure. The quantity of the employed starting materials is reported in Table 1. As per the chemical formulae, the stoichiometric quantities of strontium nitrate ( $\text{Sr}(\text{NO}_3)_2$ ) (Sigma-Aldrich, purity: 99%), zirconium nitrate oxide dihydrate ( $\text{ZrO}(\text{NO}_3)_2 \cdot 2\text{H}_2\text{O}$ ) (Kanto chemical, purity: 99%), holmium(III) nitrate pentahydrate ( $\text{Ho}(\text{NO}_3)_3 \cdot 5\text{H}_2\text{O}$ ) (Sigma-Aldrich, purity: 99.9%), citric acid ( $\text{C}_6\text{H}_8\text{O}_7$ ) (Junsei, purity: 99.5%) and, a mixture of 6 ml of ethanol and 4 ml of water combine in a 150 ml beaker. The molar ratio was kept at 2 : 1 according to citric acid and total metal ions. Next, the mixture was stirred for 1 h to achieve a clear homogeneous solution; after that, put the resultant in the oven until the solution dried. A hot temperature furnace maintained at 400 °C preheated the acquired gels for 2 h in air. After preheating, the samples were granulated and fired for 4 h at 1050 °C in the ambient condition, giving the fine powder samples. Fig. 1 presents a pictorial view of the synthesis process.

The X-ray diffraction patterns were monitored by a RIGAKU (Miniflex-II) diffractometer attached to an X-ray source (Cu-K $\alpha$  radiation,  $\lambda = 1.5406 \text{ \AA}$ ); the scan rate was set at 5° per minute between 10°–80° for 2 $\theta$  angle. To identify the functional group present in the prepared samples, a Fourier transform infrared (6700, Thermo Fisher Nicolet) spectrometer was operated in a range of 400–4000  $\text{cm}^{-1}$ . A small quantity of prepared  $\text{SrZrO}_3:\text{Ho}^{3+}$  phosphor powder is used to measure diffuse reflectance with A Cary-5000 (UV-VIS-NIR) spectrophotometer coupled to a Praying Mantis diffuse reflectance accessory. Photoluminescence (PL) spectra were analyzed by a Shimadzu (RF-5301PC) spectrofluorophotometer fitted with a Xenon-flash lamp. The emission and excitation spectra were recorded using a spectral slit width of 1.5 nm. The above characterizations were performed at room temperature.

## 3. Results and discussion

### 3.1 Crystal structure

The XRD measurement was conducted to study the structural phase and crystallinity of the prepared samples. Fig. 2 displays the XRD patterns of the  $\text{SrZrO}_3:x\text{Ho}^{3+}$  powders. For the synthesized phosphors, the major diffraction peaks matched with JCPDS (Joint Committee for Powder Diffraction Standards Card) File No. 76-0167 corresponding to  $\text{SrZrO}_3$ . The effect of  $\text{Ho}^{3+}$  ions (at the studied concentrations *i.e.* 0.01, 0.03, 0.05, 0.07, 0.09, and 0.11 mol) on the structure of the  $\text{SrZrO}_3$  lattice seems to be negligible as XRD patterns remain the almost same at different doping concentrations. However, we believe the actual doping level can be clarified by Le Bail method to find the evolution trend of the cell lattice parameters. To calculate the crystalline size, the FWHM (full width at half maximum) of dominant (110) diffraction peaks are considered in leading Scherrer's equation,  $D = 0.9\lambda/\beta \cos \theta$ , in which the wavelength of incident X-rays is denoted as  $\lambda$ , the corresponding Bragg's diffraction angle is  $\theta$ , and the FWHM of the (110) peak is  $\beta$ . The

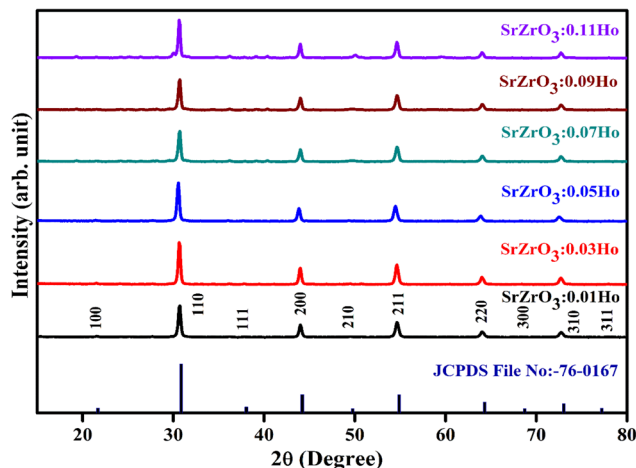


Fig. 2 Powder XRD patterns of  $\text{SrZrO}_3:x\text{Ho}^{3+}$  phosphors.

determined crystal sizes were approximately within the range of 24–31 nm. Various oxides with the  $\text{ABO}_3$  chemical formula follow the perovskite structure. Fig. 3 showed the simplified crystal lattice of the  $\text{SrZrO}_3$  perovskite. The  $\text{SrZrO}_3$  has cubic symmetry with a  $Pm\bar{3}m[221]$  space group. In the  $\text{SrZrO}_3$  perovskite structure, the Sr atoms are situated on the edges of the cubic unit cell, and the 12 closest neighbor O atoms surround the Sr atoms. Similarly, the Zr atom is situated in the centrum of the unit cell and is six-fold integrated with the O closed-neighbor atoms, making an octahedron. The cubic unit cell faces have O atoms, which are two-fold coordinated with Zr neighbor atoms. The Zr-ion and Sr-ion have the coordination numbers 6 and 8, respectively.<sup>1,11</sup>

### 3.2 Vibrational analysis

Fig. 4 shows a typical vibrational feature of the  $\text{SrZrO}_3:0.03\text{Ho}^{3+}$  powder sample. An intense absorption band at 558  $\text{cm}^{-1}$  is attributed to the Zr–O stretching vibration. We have also observed a sharp peak at 857  $\text{cm}^{-1}$ . Katyayan and Agrawal<sup>18</sup> studied  $\text{SrZrO}_3:\text{Eu}^{3+}, \text{Tb}^{3+}$  system and several peaks reported in the range of 509–895  $\text{cm}^{-1}$  were due to the vibrational stretching modes of metal–oxygen bond, *i.e.*, Zr–O bond. However, few peaks lie between 1000 and 1270  $\text{cm}^{-1}$  due to the active modes of asymmetric stretching of impurity ions. Further, sharp peaks were reported within 1302–1588  $\text{cm}^{-1}$  due to the symmetrical stretching of Sr–O bonds. We have also observed bands at 1018 and 1458  $\text{cm}^{-1}$ . The observed bands and their assignments can be confirmed with the previous literature.<sup>8,38–41</sup>

### 3.3 Diffuse reflectance spectra and optical band gap

The UV-diffuse reflectance spectra were recorded between the wavelength regions of 200–800 nm for the 3 mol%  $\text{Ho}^{3+}$  doped  $\text{SrZrO}_3$  phosphor. Fig. 5 shows the diffuse reflectance spectrum and extracted absorption coefficient with the Kubelka–Munk function. It can be seen that few bands around 365, 421, 454, 468, 489, 542, and 645 nm are related to the 4f–4f configuration of  $\text{Ho}^{3+}$  transitions:  $^5\text{I}_8 \rightarrow ^5\text{G}_5 + ^3\text{H}_6, ^5\text{I}_8 \rightarrow ^5\text{G}_5, ^5\text{I}_8 \rightarrow ^5\text{G}_6, ^5\text{I}_8 \rightarrow$



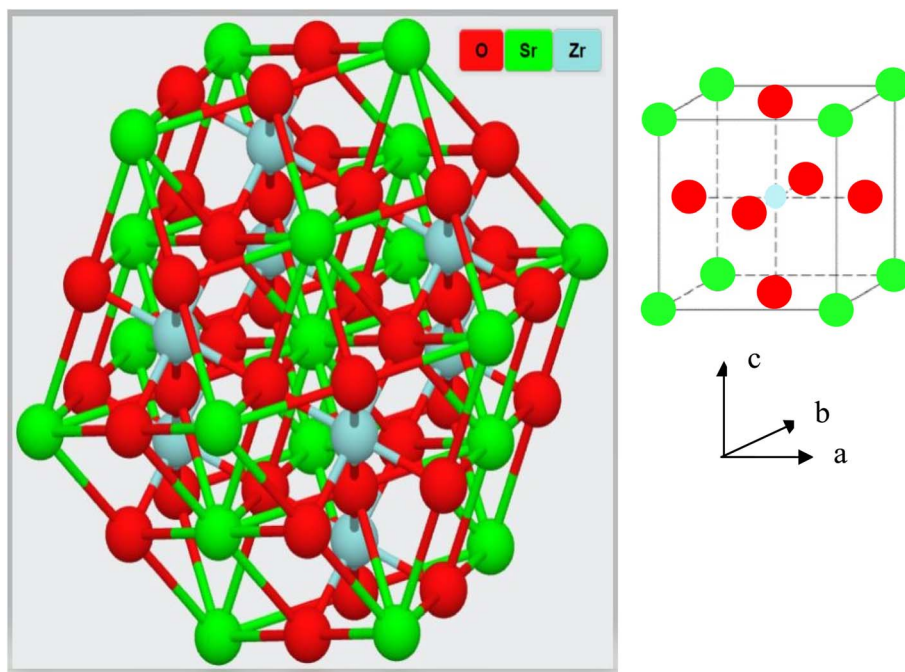


Fig. 3 Crystal structure of the SrZrO<sub>3</sub> perovskite.

$^5F_1$ ,  $^5I_8 \rightarrow ^5F_2 + ^3K_8$ , and  $^5I_8 \rightarrow ^5F_3$ , respectively. The extracted optical-absorption coefficient ( $\alpha \text{ cm}^{-1}$ ) was calculated by the consecutive expression:<sup>42</sup>

$$F(R) = \frac{(1 - R)^2}{2R} = \alpha \quad (1)$$

where  $R$  stands for sample reflectance. The  $E_g$  (optical band gaps) for the Ho<sup>3+</sup> doped SrZrO<sub>3</sub> phosphor can be estimated with the Tauc relation:<sup>43</sup>

$$F(R)\hbar\omega \approx A(\hbar\omega - E_g)^n \quad (2)$$

where  $A$  is a constant,  $F(R)$  is the absorption coefficient with photon energy ( $\hbar\omega$ ) and  $n$  represents the power factor:  $n = 1/2$  allowed direct transitions, and  $n = 2$  allowed an indirect transition. Fig. 6 shows plots of  $(F(R)\hbar\omega)^n$  as a function of  $\hbar\omega$  (eV). After assuming  $(F(R)\hbar\omega)^2 = 0$  and  $(F(R)\hbar\omega)^{1/2} = 0$  for the linear region within the plot, the energy band gaps of the direct allowed and indirectly allowed transitions were observed to be 5.21 eV and 5.43 eV, correspondingly for the SrZrO<sub>3</sub>:0.03Ho<sup>3+</sup> phosphor.

### 3.4 Photoluminescence analysis

Fig. 7(a) demonstrates the photoluminescence excitation (PLE) spectra for the produced Ho<sup>3+</sup> doped SrZrO<sub>3</sub> phosphors. The

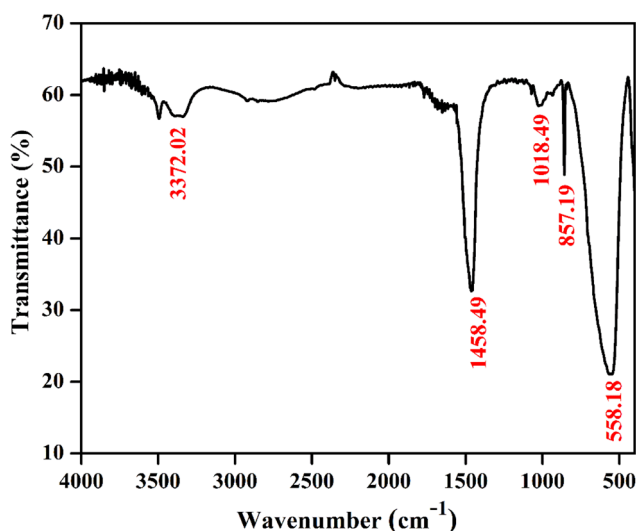


Fig. 4 FTIR spectrum of SrZrO<sub>3</sub>:0.03Ho<sup>3+</sup> phosphor.

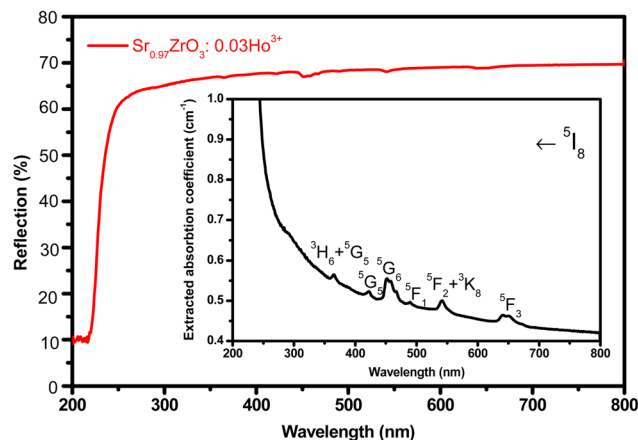


Fig. 5 UV-visible diffuse reflectance spectrum of SrZrO<sub>3</sub>:0.03Ho<sup>3+</sup> phosphor. Inset of the figure shows extracted absorption spectrum.



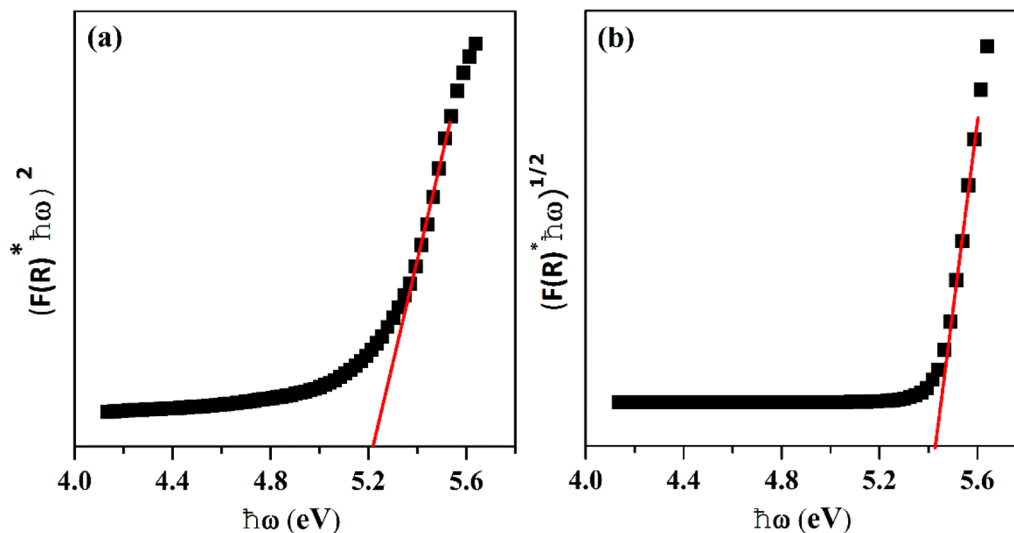


Fig. 6 Plots of  $(F(R)\hbar\omega)^n$  versus  $\hbar\omega$  (eV): (a) direct allowed transition and (b) indirect allowed transition.

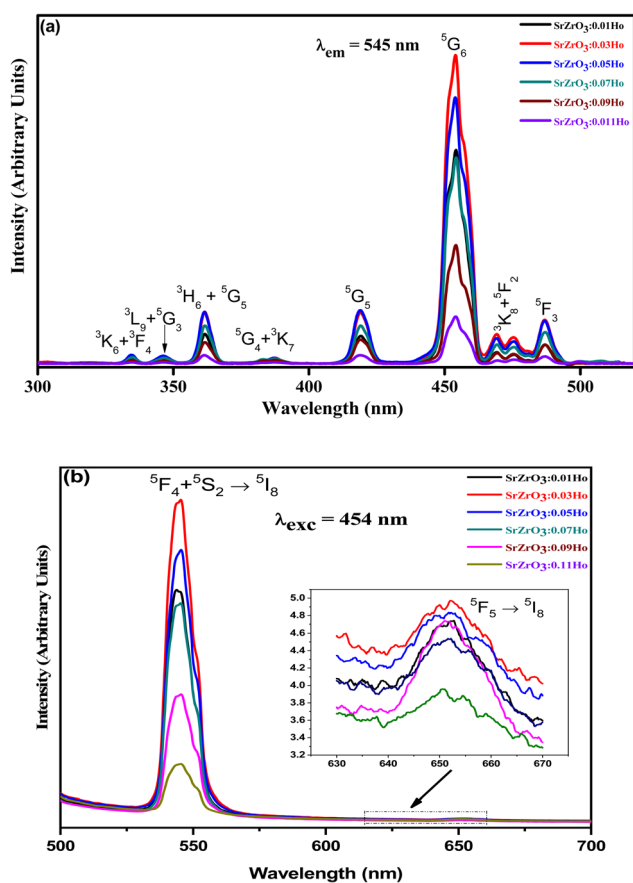


Fig. 7 (a) Photoluminescence excitation spectra of  $\text{SrZrO}_3:\text{xHo}^{3+}$  phosphors ( $\lambda_{\text{em}} = 545$  nm) and (b) photoluminescence emission spectra of  $\text{SrZrO}_3:\text{xHo}^{3+}$  phosphors ( $\lambda_{\text{exc}} = 454$  nm).

PLE spectra were acquired using the emission band at 545 nm. It can be read that the narrow bands owing to the  $4f-4f$  transitions of  $\text{Ho}^{3+}$  ions and originated from  $^5\text{I}_8$  to  $^3\text{K}_6 + ^3\text{F}_4$  (334 nm),  $^3\text{L}_9 + ^5\text{G}_3$  (346 nm),  $^3\text{H}_6 + ^5\text{G}_5$  (361 nm),  $^3\text{K}_7 + ^5\text{G}_4$  (387 nm),  $^5\text{G}_5$

(418 nm),  $^5\text{G}_6$  (454 nm),  $^5\text{F}_2 + ^3\text{K}_8$  (472 nm) and  $^5\text{F}_3$  (486 nm). The highest PLE intensity was observed at 454 nm; this would be suitable as the excitation wavelength for all prepared phosphors. The PLE band intensity is saturated at 3 mol% of  $\text{Ho}^{3+}$  ions in the  $\text{SrZrO}_3$  phosphor. Usually, the doping of  $\text{Ho}^{3+}$  ions in place of  $\text{Sr}^{2+}$  ions will create positive charge defects that would negatively affect luminescence. Therefore, the expected emission intensity is maximum for 3 mol% of  $\text{Ho}^{3+}$  ions, and then the subsequent decrease of emission intensity is due to the  $\text{Ho}_{\text{Sr}^{2+}}$  defects.<sup>44</sup>

The emission spectra were monitored using 454 nm as the excitation wavelength for all phosphors and are presented in

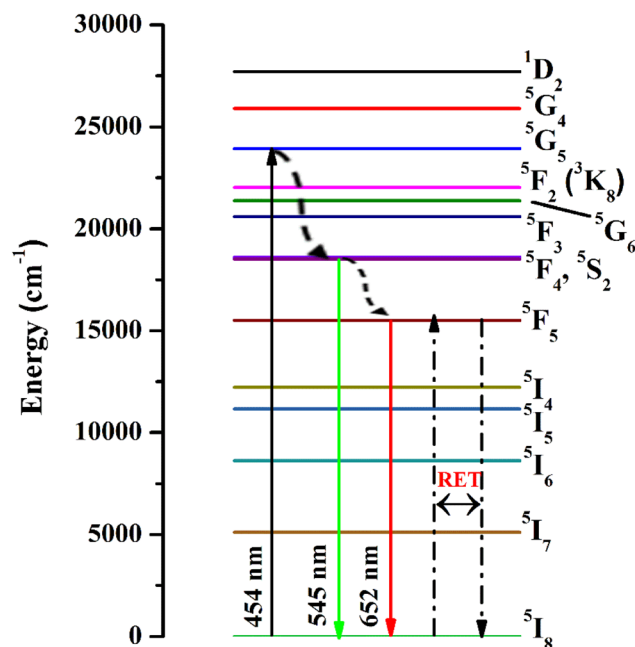


Fig. 8 Schematic energy level diagram for  $\text{Ho}^{3+}$  ions with possible radiative and non-radiative transitions.



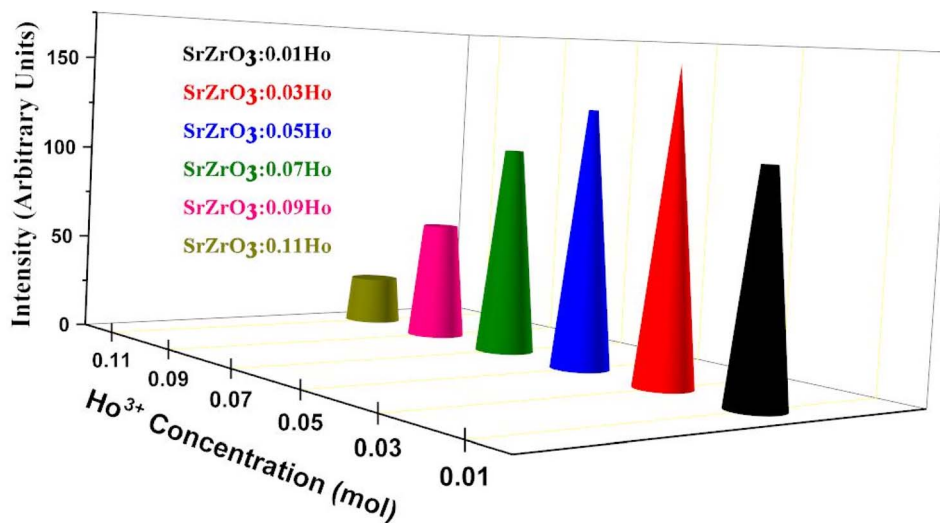


Fig. 9 Variation of emission intensity ( $I_{545 \text{ nm}}$ ) as a function of  $\text{Ho}^{3+}$  ions in the  $\text{SrZrO}_3:\text{Ho}^{3+}$  phosphor.

Fig. 7(b). Strong green and weak red emission bands have been seen around 545 nm and 652 nm. The obtained bands are possibly defined as transitions of  $\text{Ho}^{3+}$  ions for  $^5\text{F}_4 + ^5\text{S}_2 \rightarrow ^5\text{I}_8$  and  $^5\text{F}_5 \rightarrow ^5\text{I}_8$ , respectively. The intensity of green emission at 545 nm is  $\sim 35$  times more substantial than the red emission at 652 nm. Upon excitation of 454 nm, the ions are excited from  $^5\text{I}_8$  to  $^5\text{G}_4$ , then most of the excited ions decay the lower levels  $^5\text{F}_4 + ^5\text{S}_2$  and  $^5\text{F}_5$  levels non-radiatively, and subsequently, radiatively transit to  $^5\text{I}_8$  level with emission of green ( $^5\text{F}_4 + ^5\text{S}_2 \rightarrow ^5\text{I}_8$ ) and red ( $^5\text{F}_5 \rightarrow ^5\text{I}_8$ ), respectively. The energy gap difference for the  $^5\text{F}_4$  and  $^5\text{F}_5$  to the next lower levels are around  $3400 \text{ cm}^{-1}$  and  $2400 \text{ cm}^{-1}$ , thus the observed difference of green and red emission intensities depends on the population of excited states and multiphonon relaxation rates ( $W_{\text{mpr}}$ ) since the  $W_{\text{mpr}}$  is increasing with the decrease of the energy gap between excited state to the next lower state. Fig. 8 shows a schematic energy level diagram for  $\text{Ho}^{3+}$  ions with possible radiative and non-radiative relaxation processes.

As seen in Fig. 9, the highest emission intensity was noticed when the  $\text{Ho}^{3+}$  ions concentration was 3 mol%, and it was decreased according to the increasing concentration of  $\text{Ho}^{3+}$  ions in the  $\text{SrZrO}_3$  phosphor because of concentration quenching. Generally, it is recognized that the Ho–Ho distance reduces with an enhancement of  $\text{Ho}^{3+}$  ion concentration, leading to fluorescence quenching that comes from an increase in the resonant transfer probability between  $\text{Ho}^{3+}$  ions. The chances of energy transmission distance between Ho–Ho ions are termed the critical distance ( $R_c$ ) obtained by the Blasse expression:<sup>45</sup>

$$R_c \approx 2 \left[ \frac{3V}{4\pi\chi_c N} \right]^{1/3} \quad (3)$$

where  $V$  is the unit cell volume, critical ion concentration is  $\chi_c$  and  $N$  is the number of Zr ions of a unit cell. For our  $\text{Ho}^{3+}$  doped  $\text{SrZrO}_3$  phosphor,  $V = 552.175 \text{ (\AA)}^3$ ,<sup>46</sup>  $N = 4$ , and  $\chi_c = 0.03$ . The calculated critical transfer distance ( $R_c$ ) is  $\sim 20 \text{ \AA}$ , far greater than  $5 \text{ \AA}$  that favors exchange interaction; thus, it can be

established that the observed concentration quenching in  $\text{Ho}^{3+}$  doped  $\text{SrZrO}_3$  samples is attributed to the multipole–multipole interaction.<sup>42</sup> In addition, the interaction strength can also be calculated using the following equation:<sup>47</sup>

$$\frac{1}{x} = K \left\{ 1 + \beta(x)^{Q/3} \right\}^{-1} \quad (4)$$

where  $K$  and  $\beta$  are constants,  $I$  is emission intensity, and  $x$  is activator ion concentration. The dipole–dipole (d–d), dipole–quadrupole (d–q), quadrupole–quadrupole (q–q) interactions take place with  $Q = 6, 8$ , and  $10$ , respectively. Fig. 10 shows the  $\log(I/x)$  based on  $\log(x)$  for the  $\text{SrZrO}_3:0.03\text{Ho}^{3+}$  phosphor. It can be observed that  $-Q/3 = -2.24$ , so  $Q = 6.72$ . Thus, the quenching in emission intensity of  $\text{Ho}^{3+}$  doped  $\text{SrZrO}_3$  host lattices is due to dipole–dipole interactions. The concentration quenching of  $\text{Ho}^{3+}$  doped  $\text{SrZrO}_3$  phosphor that occurred beyond the optimized concentration (3 mol%) is most useful for emitting green light in optoelectronic devices.

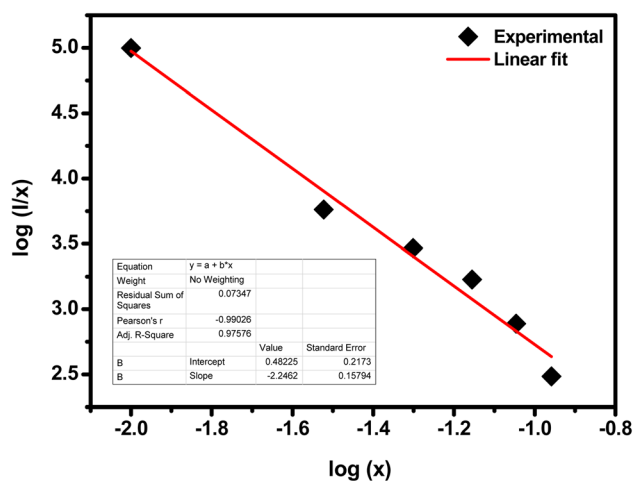


Fig. 10 Plot of  $\log(I/x)$  as a function of  $\log(x)$  of the  $\text{SrZrO}_3:0.03\text{Ho}^{3+}$  phosphor (where  $I$  is the green emission peak intensity, and  $x$  is the  $\text{Ho}^{3+}$  ion concentration).



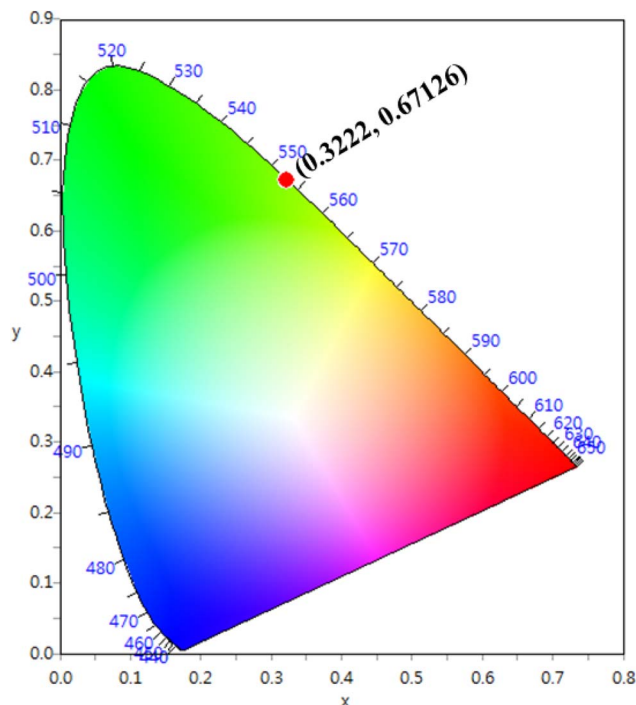


Fig. 11 CIE chromaticity diagram of SrZrO<sub>3</sub>:0.03Ho<sup>3+</sup> phosphor.

The CIE chromaticity coordinates were determined by the emission spectrum ( $\lambda_{\text{exc}} = 454 \text{ nm}$ ) of optimized Ho<sup>3+</sup> (3 mol%) doped SrZrO<sub>3</sub> phosphor using 1931 CIE (Commission International de l'Eclairage France) technology, which is an accepted standard for the LED industry in matters related to colors, such as color mixing and color rendering. The chromaticity coordinates were found to be (0.322, 0.671) and this is situated in the green region of the CIE chromaticity diagram (see Fig. 11). The correlated color temperature (CCT) was also estimated by the McCamy experimental equation:<sup>48</sup>

$$\text{CCT} = -437n^3 + 3601n^2 - 6861n + 5514.31 \quad (5)$$

where  $n = \frac{(x - x_e)}{(y - y_e)}$  with chromaticity epicenter being  $x_e = 0.3320$  and  $y_e = 0.1858$ . The obtained CCT is 5654 K for the Ho<sup>3+</sup> (3 mol%) doped SrZrO<sub>3</sub> phosphor. Thus, this could be useful for w-LEDs because a CCT < 5000 K gives warm-white LEDs for home gadgets.

### 3.5 Judd–Ofelt intensity parameters from PLE and radiative properties

The familiar Judd–Ofelt intensity parameters ( $\Omega_\lambda$  with  $\lambda = 2, 4$ , and 6) were adopted to figure out the fluorescence branching ratios, spontaneous emission probabilities, and radiative lifetimes of the excited multiplets to assess the undertaking of lasers and luminescent materials. As per Judd–Ofelt (J–O) theory,<sup>49,50</sup> the J–O intensity parameters ( $\Omega_\lambda$  with  $\lambda = 2, 4$ , and 6) can be examined conventionally from absorption spectra by evaluating the measured and computed spectral line strengths of the excited 4f–4f electronic transitions using least-square or chi-square fit methods. However, in recent decades,<sup>42,51,52</sup>

Table 2 Doubly reduced matrix elements  $\|U^2\|^4$  ( $\lambda = 2, 4$  and 6), relative line strengths ( $S^{\text{rel}}$ ) ( $\times 10^{-20} \text{ cm}^2$ ) for the observed excitation/absorption bands of Ho<sup>3+</sup> doped various host matrices

Transitions from $^5I_8 \rightarrow$	Excitation band wavenumber ( $\nu \text{ cm}^{-1}$ )	<sup>a</sup> SrZrO <sub>3</sub> :0.03Ho <sup>3+</sup>		YLIF <sup>55</sup>		GdLiF <sub>4</sub> (ref. 55)		LuLiF <sub>4</sub> (ref. 55)	
		$\ U^2\ ^4$	$S^{\text{rel}}$	$\ U^2\ ^4$	$S^{\text{rel}}$	$\ U^2\ ^4$	$S^{\text{rel}}$	$\ U^2\ ^4$	$S^{\text{rel}}$
<sup>3</sup> K <sub>6</sub> + <sup>3</sup> F <sub>4</sub>	29 922	0.0073	0.024	0.309	0.341	0.309	0.251	0.309	0.251
<sup>3</sup> L <sub>9</sub> + <sup>5</sup> G <sub>3</sub>	28 902	0.1263	0.031	0.394	0.379	0.394	0.300	0.394	0.300
<sup>3</sup> H <sub>6</sub> + <sup>3</sup> H <sub>5</sub>	27 685	0.0052	0.173	1.310	4.377	1.310	1.276	1.310	1.276
<sup>5</sup> G <sub>4</sub> + <sup>3</sup> K <sub>7</sub>	25 846	0.2337	0.021	0.325	0.345	0.325	0.307	0.325	0.307
<sup>5</sup> G <sub>5</sub>	23 872	0.0361	0.085	1.161	1.199	1.161	1.120	1.161	1.120
<sup>5</sup> G <sub>6</sub>	22 020	0.5338	0.085	3.893	4.177	3.893	4.014	3.893	4.014
<sup>5</sup> F <sub>2</sub> + <sup>3</sup> K <sub>6</sub>	21 186	0.8410	0.791	0.392	0.446	0.392	0.248	0.392	0.248
<sup>5</sup> F <sub>3</sub>	20 542	0.0334	0.083	0.716	0.811	0.716	0.375	0.716	0.375
$\delta_{\text{rms}}$		0	0.067	± 0.117	± 0.114	± 0.117	± 0.108	± 0.117	± 0.108

<sup>a</sup> Present work.

a simple approach has been proposed to evaluate J–O intensity parameters from the assessment of excitation spectra. This approach is successfully applied to Nd<sup>3+</sup>, Er<sup>3+</sup> and Dy<sup>3+</sup> doped various phosphor powders.

Normally, the excitation and absorption spectral difference lies in the intensity ratio of the fluorescence excitation to the absorption (*i.e.*, relative fluorescence quantum efficiency). Therefore, the excitation and absorption spectra will coincide exactly while relative fluorescence quantum efficiency maintains to be constant at different wavelengths. Once the experimental excitation spectrum is corrected to the corresponding absorption spectrum in which the excited states are followed by a very fast non-radiative relaxation to the monitored level.<sup>53,54</sup> In this work, the excited multiplets of Ho<sup>3+</sup>: <sup>5</sup>G<sub>5</sub>, <sup>5</sup>F<sub>2</sub>(<sup>3</sup>K<sub>8</sub>), <sup>5</sup>G<sub>6</sub>, <sup>5</sup>F<sub>3</sub> levels are nonradiatively relaxed to <sup>5</sup>F<sub>4</sub> + <sup>5</sup>S<sub>2</sub> monitored level may satisfy the above statement, and excited multiplets chosen as ideal ones for the determination Judd–Ofelt parameters. The calculated and measured relative excited line strength for the attended electric-dipole transitions across the *aJ* and *bJ'* levels are determined using the following expressions,<sup>55,56</sup>

$$S_{\text{cal}}^{\text{ed}}(aJ; bJ') = \sum_{\lambda=2,4,6} \Omega_{\lambda} |\langle [\alpha SL]J \| U^{(\lambda)} \| [\alpha' S' L']J' \rangle|^2 \quad (6)$$

$$S_{\text{meas}}^{\text{ed}}(aJ; bJ') = \frac{3\text{ch}(2J+1)}{8\pi^3 \bar{\lambda}^3 e^2 N_0} \frac{9n}{(n^2+2)^2} I_{\text{exc}} \quad (7)$$

where  $\Omega_{\lambda}$  is the J–O intensity parameter, which is used in the environmental field effect of intermixing states, *i.e.*, 4f<sup>N</sup>–15d and 4f<sup>N</sup>–15g.  $U^{(\lambda)}$  is the doubly reduced matrix tensor operator and it is found in the coupling approximations approach, which is taken from the literature.<sup>56</sup> The term  $n \sim 2.12$  is the refractive index of SrZrO<sub>3</sub> material.<sup>57</sup> The average wavelength of the excitation band is denoted as  $\bar{\lambda}$ ,  $N_0$  is the ion concentration and  $\bar{I}$  is the integrated relative excitation intensity of each band.  $\Omega_{\lambda}$  parameters were predicted by a least square fitting technique.<sup>43</sup> Table 2 shows relative spectral line strengths of excited transitions for Ho<sup>3+</sup> ions (3 mol%) in the SrZrO<sub>3</sub> phosphor.<sup>55</sup> The root average square deviation ( $\delta_{\text{rms}}$ ) between experimental line strengths is,

$$\delta_{\text{rms}} = \sqrt{\frac{\sum (S_{\text{exp}}^{\text{ed}} - S_{\text{meas}}^{\text{ed}})^2}{(q-p)}} \quad (8)$$

where  $q$  and  $p$  are fitting parameters as transition number, and it has been used in our case as  $q = 8$  and  $p = 3$  in the best least square fitting procedure. The observed small  $\delta_{\text{rms}}$  value (see Table 2) is indicative of the validity and fit quality in J–O theory.

Table 3 describes the J–O intensity parameters considering various host matrices.<sup>58–62</sup> The  $\Omega_2$  parameter indicates ionicity (or covalence) of RE–O bonds and is related to the local structure.  $\Omega_4$  and  $\Omega_6$  are non-sensitive to the dependence structure and are attributed to the stiffness of the host; however, the various active ions alter the characteristics of the evaluated spontaneous emission transitions. For example, from Table 3, the Ho<sup>3+</sup> doped SrZrO<sub>3</sub> phosphor shows a lower ionic nature between Ho–O bonds compared with other oxide-based host

Table 3 Relative Judd–Ofelt intensity parameters, ( $\Omega_{\lambda} \times 10^{-20} \text{ cm}^2$ ,  $\lambda = 2, 4$  and 6) of various host matrices

Host	$\Omega_2$	$\Omega_4$	$\Omega_6$	Order
<sup>a</sup> SrZrO <sub>3</sub> :0.03Ho <sup>3+</sup>	0.41	0.16	0.19	$\Omega_6 > \Omega_4 > \Omega_2$
Y <sub>3</sub> Al <sub>5</sub> O <sub>15</sub> (YAG) <sup>58</sup>	0.04	2.67	1.89	$\Omega_4 > \Omega_6 > \Omega_2$
Lu <sub>3</sub> Al <sub>5</sub> O <sub>12</sub> (ref. 59)	0.17	2.08	1.92	$\Omega_4 > \Omega_6 > \Omega_2$
LaF <sub>3</sub> (ref. 60)	1.16	1.38	0.88	$\Omega_2 > \Omega_4 > \Omega_6$
LiYF <sub>4</sub> (ref. 61)	1.01	1.71	1.21	$\Omega_4 > \Omega_6 > \Omega_2$
LiYF <sub>4</sub> (ref. 62)	0.96	2.05	1.43	$\Omega_4 > \Omega_6 > \Omega_2$

<sup>a</sup> Present work.

matrices. On the other hand, when compared with a fluoride-based host, the Ho<sup>3+</sup> doped SrZrO<sub>3</sub> phosphor shows a higher ionic nature between the Ho–O bonds because of the lesser values of the J–O intensity parameter,  $\Omega_2$ .

## 4. Conclusions

The SrZrO<sub>3</sub>:Ho<sup>3+</sup> phosphors were produced by a sol–gel system and were analyzed by X-ray diffraction, FTIR, UV-visible and photoluminescence spectroscopic techniques. We have identified absorption bands around 365, 421, 454, 468, 489, 542, and 645 nm from the UV-visible diffuse reflectance spectrum of the 4f–4f configuration of Ho<sup>3+</sup> transitions. The optical band gaps ( $E_{\text{opt}}$ ) were found to be 5.21 eV (direct transition), 5.43 eV (indirect transition), respectively for the Ho<sup>3+</sup> doped SrZrO<sub>3</sub> phosphor. Upon 454 nm excitation, the Ho<sup>3+</sup> doped SrZrO<sub>3</sub> phosphor exhibits high green and low red emission bands that are connected to the respective <sup>5</sup>F<sub>4</sub> + <sup>5</sup>S<sub>2</sub> → <sup>5</sup>I<sub>8</sub> (545 nm) and <sup>5</sup>F<sub>5</sub> → <sup>5</sup>I<sub>8</sub> (652 nm) transitions of Ho<sup>3+</sup> ions. The fluorescence quenching of the studied phosphor samples was evaluated by looking at the critical distance between Ho–Ho ions as well as the strength of dipole–dipole (d–d), dipole–quadrupole (d–q) and quadrupole–quadrupole (q–q) interactions. The obtained CCT was 5654 K for the optimum concentration of Ho<sup>3+</sup> (3 mol%) doped in the SrZrO<sub>3</sub> phosphor suggesting that it may be useful for w-LEDs. In addition, using excitation spectrum of the optimized phosphor, the Judd–Ofelt intensity parameters ( $\Omega_{\lambda}$  with  $\lambda = 2, 4$  and 6) for Ho<sup>3+</sup> were estimated and compared with other hosts. The observed results of photoluminescence properties suggested that the SrZrO<sub>3</sub>:0.03Ho<sup>3+</sup> phosphor may be advantageous for green emitting optoelectronic applications.

## Conflicts of interest

There are no conflicts to declare.

## Acknowledgements

This work was supported by the National Research Foundation of Korea (NRF) grant funded by the Korea government (MSIT) (2018M2B2A9065656). This paper was also supported by the KU Research Professor Program of Konkuk University.



## References

- 1 S. K. Gupta, A. K. Yadav, D. Bhattachary, S. N. Jha and V. Natarajana, Visible light emitting  $\text{Ln}^{3+}$  ion ( $\text{Ln}=\text{Sm}$ ,  $\text{Eu}$  and  $\text{Dy}$ ) as a structural probe: A case study with  $\text{SrZrO}_3$ , *J. Lumin.*, 2015, **164**, 1–22.
- 2 K. Nonaka, M. Akiyama, C.-N. Xu, T. Hagio, M. Komatsu and A. Takase, Enhanced photovoltaic response in lead lanthanum zirconate-titanate ceramics with A-Site deficient composition for photostrictor application, *Jpn. J. Appl. Phys.*, 2000, **39**, 9A.
- 3 E. Caetano, C. Souza and R. Muccillo, Properties and applications of perovskite proton conductors, *Mater. Res.*, 2010, **13**, 385–394.
- 4 M. Kubicek, A. H. Bork and J. L. M. Rupp, Perovskite oxides - a review on a versatile material class for solar-to-fuel conversion processes, *J. Mater. Chem. A*, 2017, **5**, 11983–12000.
- 5 M. Sukumar, L. John Kennedy, J. Judith Vijaya, B. Al-Najar, M. Bououdina and G. Mudhana, Structural, optical, and magnetic properties of  $\text{Ca}^{2+}$  doped  $\text{La}_2\text{CuO}_4$  perovskite nanoparticles, *Vacuum*, 2019, **167**, 407–415.
- 6 M. A. Peña and J. L. G. Fierro, Chemical structures and performance of perovskite oxides, *Chem. Rev.*, 2001, **101**, 1981–2018.
- 7 J. Etourneau, J. Portier and F. Ménil, The role of the inductive effect in solid state chemistry: how the chemist can use it to modify both the structural and the physical properties of the materials, *J. Alloys Compd.*, 1992, **188**, 1–7.
- 8 S. Katyayan and S. Agrawal, Study of optical behaviour of  $\text{Eu}^{3+}$  and  $\text{Tb}^{3+}$  doped zirconate perovskite phosphors prepared by molten salt technique, *Opt. Quantum Electron.*, 2020, **52**, 18.
- 9 N. R. Amadass,  $\text{ABO}_3$ -type oxides-Their structure and properties-a bird's eye view, *Mater. Sci. Eng.*, 1978, **36**, 231–239.
- 10 G. Pan, X. Bai, D. Yang, X. Chen, P. Jing, S. Qu, L. Zhang, D. Zhou, J. Zhu, W. Xu, B. Dong and H. Song, Doping lanthanide into perovskite nanocrystals: highly improved and expanded optical properties, *Nano Lett.*, 2017, **17**, 8005–8011.
- 11 S. K. Gupta, P. S. Ghosh, A. K. Yadav, N. Pathak, A. Arya, S. N. Jha, D. Bhattacharyya and R. M. Kadam, Luminescence properties of  $\text{SrZrO}_3/\text{Tb}^{3+}$  perovskite: host-dopant energy-transfer dynamics and local structure of  $\text{Tb}^{3+}$ , *Inorg. Chem.*, 2016, **554**, 1728–1740.
- 12 S. K. Gupta, N. Pathak and R. M. Kadam, an efficient gel-combustion synthesis of visible light emitting barium zirconate perovskite nanoceramics: probing the photoluminescence of  $\text{Sm}^{3+}$  and  $\text{Eu}^{3+}$  doped  $\text{BaZrO}_3$ , *J. Lumin.*, 2016, **169**, 106–114.
- 13 S. K. Gupta, N. Pathak, R. Gupta, S. K. Thulasidas and V. Natarajan, Probing the oxidation state and coordination geometry of uranium ion in  $\text{SrZrO}_3$  perovskite, *J. Mol. Struct.*, 2014, **1068**, 204–209.
- 14 Z. Li, H. Duan, Y. Jin, S. Zhang, Y. Lv, Q. Xu and Y. Hu, Intrinsic defects and spectral characteristics of  $\text{SrZrO}_3$  perovskite, *Phys. B*, 2018, **534**, 105–112.
- 15 K. S. Knight and C. L. Bulle, Low temperature and high pressure thermoelastic and crystallographic properties of  $\text{SrZrO}_3$  perovskite in the Pbnm phase, *Solid State Sci.*, 2016, **62**, 90–104.
- 16 A. Mai, V. A. C. Haanappel, S. Uhlenbruck, F. Tietz and D. Stöver, Ferrite-based perovskites as cathode materials for anode-supported solid oxide fuel cells: Part I. variation of composition, *Solid State Ionics*, 2005, **176**, 1341–1350.
- 17 E. Mete, R. Shaltaf and Ş. Ellialtıođlu, Electronic and structural properties of a 4d perovskite: Cubic phase of  $\text{SrZrO}_3$ , *Phys. Rev. B: Condens. Matter Mater. Phys.*, 2003, **68**, 035119.
- 18 L. Bi, S. Boulfrad and E. Traversa, Steam electrolysis by solid oxide electrolysis cells (SOECs) with proton-conducting oxides, *Chem. Soc. Rev.*, 2014, **43**, 8255–8270.
- 19 D. Souptel, G. Behr and A. M. Balbashov,  $\text{SrZrO}_3$  single crystal growth by floating zone technique with radiation heating, *J. Cryst. Growth*, 2002, **236**, 583–588.
- 20 C. J. Howard, K. S. Knight, B. J. Kennedy and E. H. Kisi, The structural phase transitions in strontium zirconate revisited, *J. Phys.: Condens. Matter*, 2000, **12**, 45.
- 21 R. E. A. McKnight, C. J. Howard and M. A. Carpenter, Elastic anomalies associated with transformation sequences in perovskites: I. Strontium zirconate,  $\text{SrZrO}_3$ , *J. Phys.: Condens. Matter*, 2000, **12**, L677–L683.
- 22 S. Yamanaka, K. Kurosaki, T. Oyama, H. Muta, M. Uno, T. Matsuda and S. -I. Kobayashi, Thermophysical properties of perovskite-type strontium cerate and zirconate, *J. Am. Ceram. Soc.*, 2005, **88**, 1496–1499.
- 23 L. Carlsson, High-temperature phase transitions in  $\text{SrZrO}_3$ , *Acta Crystallogr.*, 1967, **23**, 901–905.
- 24 J. R. Sambrano, V. M. Longo, E. Longo and C. A. Taft, Electronic and structural properties of the (001)  $\text{SrZrO}_3$  surface, *J. Mol. Struct.: THEOCHEM*, 2007, **813**, 49–56.
- 25 N. Singh, M. Seshadri, M. S. Pathak and V. Singh, Structural and photoluminescence properties of orange emitting perovskites  $\text{SrZrO}_3:\text{Sm}^{3+}$  phosphors for solid-state lighting, *Solid State Sci.*, 2019, **87**, 163–170.
- 26 R. Lisiecki, M. Głowacki, M. Berkowski and W. Rybar-Romanowski, Contribution of energy transfer processes to excitation and relaxation of  $\text{Yb}^{3+}$  ions in  $\text{Gd}^+(\text{Al,Ga})_5\text{O}_{12}:\text{RE}^{3+}$ ,  $\text{Yb}^{3+}$  ( $\text{RE}^{3+} = \text{Tm}^{3+}$ ,  $\text{Er}^{3+}$ ,  $\text{Ho}^{3+}$ ,  $\text{Pr}^{3+}$ ), *J. Lumin.*, 2019, **211**, 54–61.
- 27 T. V. Gavrilović, D. J. Jovanović, K. Smits and M. D. Dramićanin, Multicolor upconversion luminescence of  $\text{GdVO}_4:\text{Ln}^{3+}/\text{Yb}^{3+}$  ( $\text{Ln}^{3+} = \text{Ho}^{3+}$ ,  $\text{Er}^{3+}$ ,  $\text{Tm}^{3+}$ ,  $\text{Ho}^{3+}/\text{Er}^{3+}/\text{Tm}^{3+}$ ) nanorods, *Dyes Pigm.*, 2016, **126**, 1–7.
- 28 H. Huang, H. Zhou, J. Zhou, T. Wang, D. Huang, Y. Wu, L. Sun, G. Zhou, J. Zhana and J. Hu, Enhanced anti-stocks luminescence in  $\text{LaNbO}_4:\text{Ln}^{3+}$  ( $\text{Ln}^{3+} = \text{Yb}^{3+}$ ,  $\text{Er}^{3+}/\text{Ho}^{3+}/\text{Tm}^{3+}$ ) with abundant color, *RSC Adv.*, 2017, **7**, 16777–16786.
- 29 S. K. Ranjan, A. K. Soni and V. K. Rai, Enhanced green upconversion emission in  $\text{Ho}^{3+}:\text{Gd}_2\text{O}_3$  phosphor by codoping of  $\text{Yb}^{3+}$  ions, *Mater. Mater. Today: Proc.*, 2017, **4**, 5593–5598.



- 30 M. Zhongfei, H. Yihua and J. Guifang, Luminescence properties of  $\text{Eu}^{3+}$  and  $\text{Ho}^{3+}$  in  $\text{Sr}_2\text{TiO}_4$ , *J. Rare Earths*, 2012, **30**, 744–747.
- 31 W. Shi, Z. Zhang, J. Qin, Y. Zhang, Y. Liu, Y. Liu, H. Gao and Y. Mao, Interface modification by up-conversion material of  $\text{Ho}^{3+}$ - $\text{Yb}^{3+}$ - $\text{Li}^+$  tri-doped  $\text{TiO}_2$  to improve the performance of perovskite solar cells, *J. Alloys Compd.*, 2018, **754**, 124–130.
- 32 P. Hou, B. Liu, Z. Guo, P. Zhou, B. Wang and L. Zhao, Effect of Ho doping on the crystal structure, surface morphology and magnetic property of  $\text{BiFeO}_3$  thin films prepared via the sol-gel technology, *J. Alloys Compd.*, 2019, **775**, 59–62.
- 33 S. Sharif, G. Murtaza, T. Meydan, P. I. Williams, J. Cuenca, S. H. Hashimdeen and F. Shaheen, Structural, surface morphology, dielectric and magnetic properties of holmium doped  $\text{BiFeO}_3$  thin films prepared by pulsed laser deposition, *Thin Solid Films*, 2018, **662**, 83–89.
- 34 A. Hussain and B. Kumar, Intrinsic polarization and resistive leakage analyses in high performance piezo/pyroelectric Ho-doped 0.64PMN-0.36PT binary ceramic, *Adv. Powder Technol.*, 2018, **29**, 3124–3137.
- 35 R. Wurm, O. Dernovsek and P. Greil, sol-gel derived  $\text{SrTiO}_3$  and  $\text{SrZrO}_3$  coatings on SiC and C-fibers, *J. Mater. Sci.*, 1999, **34**, 4031–4037.
- 36 G. Venkatesh, B. Blessto, C. S. K. Rao, R. Subramanian and L. John Berchmans, Novel perovskite coating of strontium zirconate in Inconel substrate, *Mater. Sci. Eng.*, 2018, **314**, 012010.
- 37 C.-Y. Liu and T.-Y. Tseng, Resistance switching properties of sol-gel derived  $\text{SrZrO}_3$  based memory thin films, *J. Phys. D: Appl. Phys.*, 2007, **40**, 7.
- 38 A. Zhang, M. Lu, S. Wang, G. Zhou, S. Wang and Y. Zhou, Novel photoluminescence of  $\text{SrZrO}_3$  nanocrystals synthesized through a facile combustion method, *J. Alloys Compd.*, 2007, **433**, L7–L11.
- 39 C. Chen, W. Zhu, T. Yu, X. Chen, X. Yao and R. G. Krishnan, F. T.-I. R., structure and dielectric property investigation of strontium zirconate thin films prepared by MOD technique, *Surf. Coat. Technol.*, 2003, **167**, 245–248.
- 40 G. Cabello, L. Lillo, C. Caro, G. E. Buono-Core, B. Chornik, M. Flores, C. Carrasco and C. A. Rodriguez, Photochemical synthesis of  $\text{AZrO}_3$ -X thin films (A=Ba, Ca and Sr) and their characterization, *Ceram. Interfaces*, 2014, **40**, 7761–7768.
- 41 V. B. Reddy and P. N. Mehrotra, Infrared and thermal studies of strontium zirconyl oxalate hexahydrate, *Thermochim. Acta*, 1979, **31**, 349.
- 42 C. Shivakumara, R. Saraf and P. Halappa, White luminescence in  $\text{Dy}^{3+}$  doped  $\text{BiOCl}$  phosphors and their Judd-Ofelt analysis, *Dyes Pigm.*, 2016, **126**, 154–164.
- 43 C. R. Kesavulu, H. J. Kim, S. W. Lee, J. Kaewkhao, N. Wantana, S. Kothan and S. Kaewjaeng, Optical spectroscopy and emission properties of  $\text{Ho}^{3+}$ -doped gadolinium calcium silicoborate glasses for visible luminescent device applications, *J. Non-Cryst. Solids*, 2017, **474**, 50–57.
- 44 L. Wang, B. K. Moon, S. H. Park, J. H. Kim, J. Shi, K. H. Kim and J. H. Jeong, Photoluminescence properties, crystal structure and electronic structure of a  $\text{Sr}_2\text{CaWO}_6:\text{Sm}^{3+}$  red phosphor, *RSC Adv.*, 2015, **5**, 89290–89298.
- 45 G. Blasse, Energy transfer in oxidic phosphors, *Phys. Lett. A*, 1968, **28**, 444–445.
- 46 S. Das, S. Som, C. Y. Yang, S. Chavhan and C. H. Lu, Structural evaluations and temperature dependent photoluminescence characterizations of  $\text{Eu}^{3+}$  activated  $\text{SrZrO}_3$  hollow spheres for luminescence thermometry applications, *Sci. Rep.*, 2016, **6**, 25787.
- 47 L. G. V. Uitert, Characterization of energy transfer interactions between rare earth ions, *J. Electrochem. Soc.*, 1967, **114**, 1048–1053.
- 48 X. C. S. McCamy, Correlated color temperature as an explicit function of chromaticity coordinates, *Color Res. Appl.*, 1992, **17**, 142–144.
- 49 B. R. Judd, Optical absorption intensities of rare-earth ions, *Phys. Rev.*, 1962, **127**, 750.
- 50 G. S. Ofelt, Intensities of crystal spectra of rare-earth ions, *J. Chem. Phys.*, 1962, **37**, 511.
- 51 W. Luo, J. Liao, R. Li and X. Chen, Determination of Judd-Ofelt intensity parameters from the excitation spectra for rare-earth doped luminescent materials, *Phys. Chem.*, 2010, **12**, 3276.
- 52 S. Dutta, S. Som and S. K. Sharma, Excitation spectra and luminescence decay analysis of  $\text{K}^+$  compensated  $\text{Dy}^{3+}$  doped  $\text{CaMoO}_4$  phosphors, *RSC Adv.*, 2015, **5**, 7380–7387.
- 53 X. Y. Chen, M. P. Jensen and G. K. Liu, Analysis of energy level structure and excited-state dynamics in a  $\text{Sm}^{3+}$  complex with soft-donor ligands:  $\text{Sm}(\text{Et}_2\text{Dtc})_3(\text{bipy})$ , *J. Phys. Chem. B*, 2005, **109**, 13991.
- 54 X. Y. Chen, E. Ma and G. K. Liu, Energy levels and optical spectroscopy of  $\text{Er}^{3+}$  in  $\text{Gd}_2\text{O}_3$  nanocrystals, *J. Phys. Chem. C*, 2007, **111**, 10404.
- 55 B. M. Walsh, G. W. Grew and N. P. Barnes, Energy levels and intensity parameters of  $\text{Ho}^{3+}$  ions in  $\text{GdLiF}_4$ ,  $\text{YLiF}_4$  and  $\text{LuLiF}_4$ , *J. Phys.: Condens. Matter*, 2005, **17**, 7643–7665.
- 56 W. T. Carnall, H. Crosswhite and H. M. Crosswhite, Energy level structure and transition probabilities in the spectra of the trivalent lanthanides in  $\text{LaF}_3$ , *Argonne National Laboratory Report*, 1977.
- 57 R. D. Shannon, R. C. Shannon, O. Medenbach and R. X. Fischer, Refractive index and dispersion of fluorides and oxides, *J. Phys. Chem. Ref. Data*, 2002, **31**, 931–970.
- 58 M. Malinowski, Z. Frukacz, M. Szufflinskaa, A. Wnuk and M. Kaczkan, Optical transitions of Ho in YAG, *J. Alloys Compd.*, 2000, **300–301**, 389–394.
- 59 D. N. Patel, B. R. Reddy and S. K. Nash-Stevenson, Spectroscopic and two-photon upconversion studies of  $\text{Ho}^{3+}$ -doped  $\text{Lu}_3\text{Al}_5\text{O}_{12}$ , *Opt. Mater.*, 1998, **10**, 225–234.
- 60 M. J. Weber, B. H. Matsinger, V. L. Dolan and G. Surratt, Optical transition probabilities for trivalent holmium in  $\text{LaF}_3$  and  $\text{YAlO}_3$ , *J. Chem. Phys.*, 1972, **57**, 562.
- 61 A. A. Kaminskii, *Crystalline lasers: physical process and operating schemes*, CRC, Florida, 1996.
- 62 C. Li, Y. Guyot, C. Linares, R. Moncorge and M. F. Joubert, Radiative transition probabilities of trivalent rare-earth ions in  $\text{LiYF}_4$ , *ASSL Proc*, 1993, **15**, 91.

